Implict SPH in LS-DYNA for Automotive Water Wading Simulations

Edouard Yreux[1]

[1]Livermore Software Technology Corporation

The explicit SPH solver implemented in LS-DYNA is well fitted for numerical simulations involving hypervelocity impacts, explosions and other transient events, but is unsuitable for slower fluid-flow simulations such as water wading. In this work, we introduce an implicit SPH formulation specifically developed for handling large-scale incompressible fluid simulations.

The method is based on a traditional projection scheme: Intermediate velocities are first predicted based on external and viscosity forces contribution, and a Poisson equation is then solved to obtain pressure forces such that incompressibility is maintained up to a given tolerance.

All the surfaces composing the structure are automatically sampled with SPH particles by LS-DYNA using a user-supplied maximum interparticle distance, and the fluid-structure interaction is embedded in the SPH solver directly. This aspect of the simulation does not require any contact card to be setup.

As the simulation evolves, the initial domain decomposition performed by LS-DYNA can become inefficient, triggering increasing communications across processors and poor load balancing, resulting in an increasing CPU time per simulation cycle as the SPH fluid particles intermix. A new feature has been developed based on the full-deck restart capability of LS-DYNA. The objective is to re-decompose the domain across processors at regular intervals, based on the updated geometry of the problem. This results in a more constant simulation time and overall improved performance.

1 Introduction

The existing SPH solver as implemented in LS-DYNA is designed to represent transient events involving extremely large deformations and material failure in solid structures under impact. It relies on an equation of state and a material model to compute material stresses, and is compatible with most materials present in LS-DYNA. Some fluid flow modeling capabilities are also available through a weakly-compressible formulation [1, 2, 3], but approximating incompressible fluids satisfactorily with this formulation requires relatively stiff equation of state parameters, which restricts the time step to a rather small value and therefore limits the efficiency of the method [4].

To more accurately represent incompressible fluids without sacrificing efficiency, an implicit incompressible SPH formulation was implemented in LS-DYNA. The method relies on a projection method [5, 6] to compute the pressure field. In a predictor phase, intermediate velocities are calculated based on external forces (such as gravity) and non-pressure internal forces (viscosity, surface tension, surface adhesion...). Pressures are then calculated through a pressure Poisson equation to correct these intermediate velocities and maintain incompressibility. While some approaches focus on correcting these intermediate velocities by reaching a divergence-free state [7], resulting inaccuracies in volume conservation are well-documented [5, 8, 9]. In this implementation, we work directly on the compression arising from these intermediate velocities, and calculate pressures to recover an incompressible state [6, 10].

The resulting formulation was implemented with large-scale problems in mind. It is therefore implemented in the massively parallel framework of LS-DYNA and has a relatively low memory footprint. The method was validated against available experimental data, and applied to large scale water wading simulations involving around 10 million particles.

2 Incompressible SPH

2.1 Incompressible SPH Formulation

The method is based on a semi-implicit Euler time integration. For all particles I, the displacements $\boldsymbol{x}_I^{n+1}$ and velocities $\boldsymbol{v}_I^{n+1}$ at time t_{n+1} are expressed as

$$\begin{cases} \boldsymbol{v}_I^{n+1} & = \boldsymbol{v}_I^n + \Delta t \frac{\boldsymbol{F}_I^n}{m_I} \\ \boldsymbol{x}_I^{n+1} & = \boldsymbol{x}_I^n + \Delta t \boldsymbol{v}_I^{n+1} \end{cases}. \tag{1}$$

The total force $\boldsymbol{F}_I^n$ acting on particle I at time t_n is first decomposed into

$$\boldsymbol{F}_I^n = \tilde{\boldsymbol{F}}_I^n + \boldsymbol{F}_{pI}^n, \tag{2}$$

where $\tilde{\boldsymbol{F}}_I^n$ contains all the forces acting on particle I other than due to internal pressure, such as gravity forces or surface tension forces, and $\boldsymbol{F}_{pI}^n$ represents the additional pressure forces that are unknown. We can compute the predicted velocities based on non-pressure forces as

$$\tilde{\boldsymbol{v}}_I^{n+1} = \boldsymbol{v}_I^n + \Delta t \frac{\tilde{\boldsymbol{F}}_I^n}{m_I}. \tag{3}$$

The density at each particle I is calculated in a typical SPH fashion with

$$\rho_I^n = \sum_J m_J W_{IJ}(t_n), \tag{4}$$

where $W_{IJ}(t_n)$ is a cubic B-Spline kernel function evaluated at $(\boldsymbol{x}_I^n - \boldsymbol{x}_J^n)$. Using a forward difference on the continuity equation $\frac{D\rho_I}{Dt} = -\rho \nabla \cdot \boldsymbol{v}$ and applying the standard SPH approximation of the divergence operator we get

$$\frac{\rho_I^{n+1} - \rho_I^n}{\Delta t} = \sum_J m_J \boldsymbol{v}_{IJ}^{n+1} \cdot \boldsymbol{\nabla} W_{IJ}(t_n), \tag{5}$$

where $\boldsymbol{v}_{IJ}^{n+1} = \boldsymbol{v}_I^{n+1} - \boldsymbol{v}_J^{n+1}$. We obtain the predicted density at t_{n+1} as

$$\tilde{\rho}_I^{n+1} = \rho_I^n + \Delta t \sum_J m_J \tilde{\boldsymbol{v}}_{IJ}^{n+1} \cdot \boldsymbol{\nabla} W_{IJ}(t_n), \tag{6}$$

where $\tilde{\boldsymbol{v}}_{IJ}^{n+1} = \tilde{\boldsymbol{v}}_I^{n+1} - \tilde{\boldsymbol{v}}_J^{n+1}$. To maintain incompressibility, we need to find the pressure forces $\boldsymbol{F}_{pI}^n$ such that $\rho_I^{n+1} = \rho_0$, where ρ_0 is the rest density of the fluid, which yields

$$\rho_0 - \tilde{\rho}_I^{n+1} = \Delta t^2 \sum_J m_J \left(\frac{\boldsymbol{F}_{pI}^n}{m_I} - \frac{\boldsymbol{F}_{pJ}^n}{m_J} \right) \boldsymbol{\nabla} W_{IJ}(t_n). \tag{7}$$

Using the regular SPH expression for pressure forces [11] we have

$$\boldsymbol{F}_{pI}^n = -m_I \sum_J m_J \left(\frac{p_I^n}{(\rho_I^n)^2} + \frac{p_J^n}{(\rho_J^n)^2} \right) \boldsymbol{\nabla} W_{IJ}^n. \tag{8}$$

Combining (7) and (8), we can obtain a linear system $\boldsymbol{A}^n \boldsymbol{p}^n = \boldsymbol{r}^n$ where p_I^n is the pressure at particle *I* at time t_n, and $r_I = \rho_0 - \tilde{\rho}_I^n$. A relaxed Jacobi solver is then employed to obtain the pressures $\boldsymbol{p}^n$ and the resulting pressure forces $\boldsymbol{F}_{pI}^n$. For more details, see [6]. Finally, we calculate the velocities and displacements at time t_{n+1} as

$$\begin{cases} \boldsymbol{v}_I^{n+1} & = \tilde{\boldsymbol{v}}_I^n + \Delta t \frac{\boldsymbol{F}_{pI}^n}{m_I} \\ \boldsymbol{x}_I^{n+1} & = \boldsymbol{x}_I^n + \Delta t \boldsymbol{v}_I^{n+1} \end{cases}. \tag{9}$$

2.2 Boundary Sampling

The fluid-structure interaction is directly handled by the SPH solver by sampling structure surfaces with SPH particles. There is no contact definition necessary between the SPH nodes and the structure surfaces. Here, we follow [12] and create boundary SPH particles that contribute to the density calculation of fluid particles. These boundary particles remain attached to the parent structure's mesh which can have arbitrary motions.

The boundary particles are created along a given triangular mesh representing the structure surfaces. Each triangle composing the structure surface mesh is sampled with SPH particles with a spacing at least as fine as the particle spacing used in the fluid discretization, to ensure the structure is watertight.

Each boundary particle K is associated with a particle volume V_K calculated as

$$V_K = \sum_{L\in\mathcal{B}} \frac{1}{W_{KL}}, \tag{10}$$

where $\mathcal{B}$ is the set containing the boundary particles. (4) becomes

$$\rho_I^n = \sum_{J\in\mathcal{F}} m_J W_{IJ}(t_n) + \sum_{K\in\mathcal{B}} \rho_0 V_K W_{IK}(t_n), \tag{11}$$

where $\mathcal{F}$ is the set containing the fluid particles. Similarly, (7) becomes

$$\rho_0 - \tilde{\rho}_I^{n+1} = \Delta t^2 \left[\sum_{J\in\mathcal{F}} m_J \left(\frac{\boldsymbol{F}_{pI}^n}{m_I} - \frac{\boldsymbol{F}_{pJ}^n}{m_J} \right) \boldsymbol{\nabla} W_{IJ}(t_n) + \sum_{K\in\mathcal{B}} \rho_0 V_K \left(\frac{\boldsymbol{F}_{pI}^n}{m_I} \right) \boldsymbol{\nabla} W_{IK}(t_n) \right] \tag{12}$$

and the total pressure force $\boldsymbol{F}_{pI}^n$ at a fluid particle I is now calculated as

$$\boldsymbol{F}_{pI}^n = -m_I \sum_{J\in\mathcal{F}} m_J \left(\frac{p_I^n}{(\rho_I^n)^2} + \frac{p_J^n}{(\rho_J^n)^2} \right) \boldsymbol{\nabla} W_{IJ}^n - m_I \sum_{K\in\mathcal{B}} \rho_0 V_K \left(\frac{p_I^n}{(\rho_I^n)^2} \right) \boldsymbol{\nabla} W_{IK}^n. \tag{13}$$

2.3 Surface Tension and Adhesion

Following [13], a surface tension force $\boldsymbol{F}_I^{\mathrm{st}}$ is calculated for each fluid particle I as

$$\frac{\boldsymbol{F}_I^{\mathrm{st}}}{m_I} = -\frac{2\rho_0}{\rho_I + \rho_J} \left[\alpha_1 \sum_{J\in\mathcal{F}} m_J \phi(|\boldsymbol{x}_I - \boldsymbol{x}_J|) \frac{\boldsymbol{x}_I - \boldsymbol{x}_J}{|\boldsymbol{x}_I - \boldsymbol{x}_J|} + \alpha_2 \sum_{J\in\mathcal{F}} (\boldsymbol{n}_I - \boldsymbol{n}_J) \right], \tag{14}$$

where α_1 and α_2 are purely numerical surface tension coefficients that need to be calibrated for different fluids,

$$\phi(r) = \frac{32}{\pi h^9} \begin{cases} 2r^3(h-r)^3 - \frac{h^6}{64} & 0 < r < \frac{h}{2} \\ r^3(h-r)^3 & \frac{h}{2} \le r < h \\ 0 & \text{otherwise} \end{cases}, \tag{15}$$

and $\boldsymbol{n}_I$ is an SPH approximation of the surface normal, calculated as

$$\boldsymbol{n}_I = h \sum_{J\in\mathcal{F}} \frac{m_J}{\rho_J} \boldsymbol{\nabla} W_{IJ}. \tag{16}$$

For modeling water, $\alpha_1 = 1.0\ \mathrm{m^4.kg^{-1}.s^{-2}}$ and $\alpha_2 = 1.0\ \mathrm{m.s^{-2}}$ have been used with some success, though a more thorough evaluation would be beneficial.

Surface adhesion between the structure and the particle is also considered, and an adhesion force $\boldsymbol{F}_I^{\mathrm{adh}}$ at a fluid particle I is calculated as [13]

$$\frac{\boldsymbol{F}_I^{\mathrm{adh}}}{m_I} = -\beta \sum_{K\in\mathcal{B}} S(|\boldsymbol{x}_I - \boldsymbol{x}_K|) \rho_0 V_K \frac{\boldsymbol{x}_I - \boldsymbol{x}_k}{|\boldsymbol{x}_I - \boldsymbol{x}_k|}, \tag{17}$$

where β is typically ranging from 0 to $1.0\ \mathrm{m^4.kg^{-1}.s^{-2}}$, and

$$S(r) = \frac{0.007}{h^{3.25}} \begin{cases} \sqrt[4]{-\frac{4r^2}{h} + 6r - 2h} & \frac{h}{2} < r < h \\ 0 & \text{otherwise} \end{cases}. \tag{18}$$

3 Input Setup in LS-DYNA

In this section, we will focus on a typical use case: an automotive water wading simulation. The problem setup is detailed here, and the results of this simulation are discussed in section 4.2.

The starting point is a set of shell parts meshed with triangular elements, representing the geometry of the car. The model is imported from a crash-test simulation, and a few additional parts are added to the model to represent sealing components omitted in the crash test model.

The vehicle is decomposed into five different rigid parts, as the various components of the car are grouped with a set of ***Deformable_To_Rigid** keywords. The first rigid part represents the main body of the car, while the other four represent each rotating wheel. The vehicle and wheels are given an initial velocity, and the front wheels have a prescribed rotational velocity to represent a front-wheel drive vehicle. The road is modeled as a flat shell, and the interaction between the vehicle and the road is captured by a contact card with a high friction coefficient.

Four ***Constrained_Joint_Revolute** keywords are added to ensure proper kinematics between the wheels and the main body of the car. Setting **lmf**=1 in ***Control_Rigid** is recommended for a more accurate representation of these joints with the relatively large time step afforded by the SPH formulation.

A rigid, fixed box-shaped shell, meshed with triangular elements, is added in front of the vehicle, to act as a container for the body of water, and a ***Define_SPH_Mesh_Box** keyword is employed to automatically generate the entire body of water inside LS-DYNA. A set of ***Define_SPH_Mesh_Surface** is also used to sample all the surfaces of the vehicle as well as the container with SPH boundary particles. Finally, the incompressible SPH formulation is activated by setting **iform**=13 in ***Control_SPH**.

The time step is controlled by a ***Define_Curve** passed as argument in the **lctm** field of ***Control_Timestep**.

LS-DYNA performs a domain decomposition across available CPUs at the beginning of the run. As the simulation evolves and the fluid particles intermix, this original decomposition can become inefficient, resulting in an increase in computational cost as more and more MPI communications are necessary. A ***Control_MPP_Decomposition_Redecomposition** keyword is added to redecompose the domain at a user-defined interval based on the current problem geometry, to restore optimal domain decomposition. A detailed overview of this feature is available in [14].

4 Numerical Examples

4.1 Validation: Dambreak and Impact

To validate the implementation of the method, we reproduce an actual dambreak experiment detailed in [15, 16]. A $1228\,\mathrm{m} \times 1000\,\mathrm{m} \times 550\,\mathrm{m}$ body of water is modeled with an interparticle distance of $10\,\mathrm{mm}$ yielding roughly $670{,}000$ particles. The containing tank and rigid box are sampled with SPH particles inside LS-DYNA. Fig. 1 illustrates the simulation at various time values, while Figs. 2 and 3 provide a comparison between SPH simulation and experimental pressure values at two different points on the rigid box surface, and shows a reasonably good agreement.

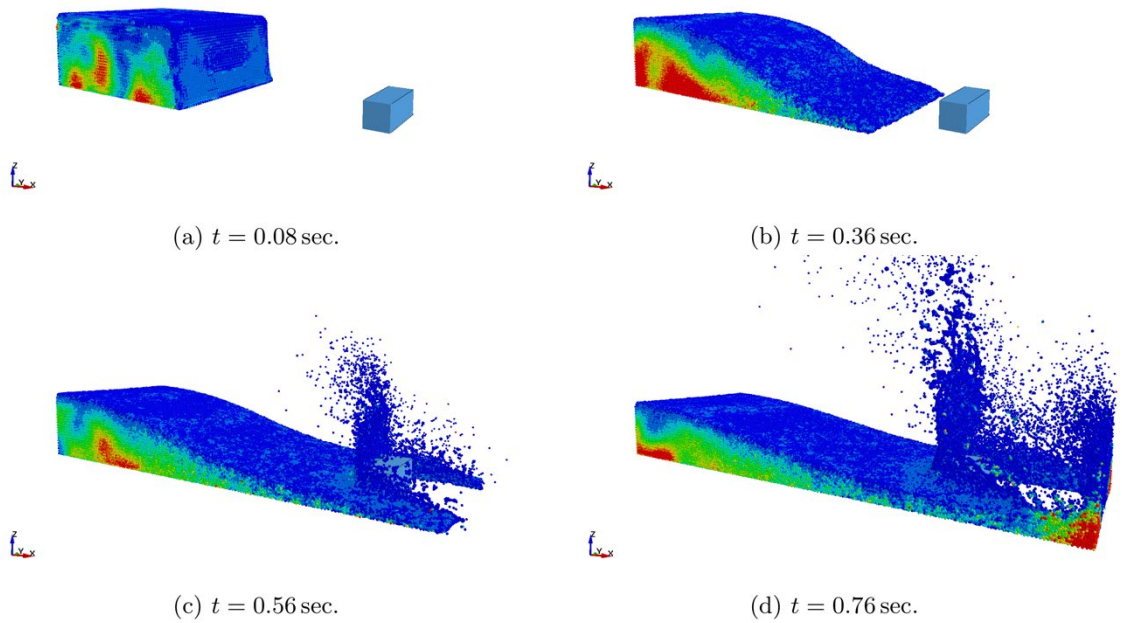

(a) $t = 0.08\,\text{sec.}$ (b) $t = 0.36\,\text{sec.}$

(c) $t = 0.56\,\text{sec.}$ (d) $t = 0.76\,\text{sec.}$

Fig.1: Dambreak simulation and impact on rigid box.

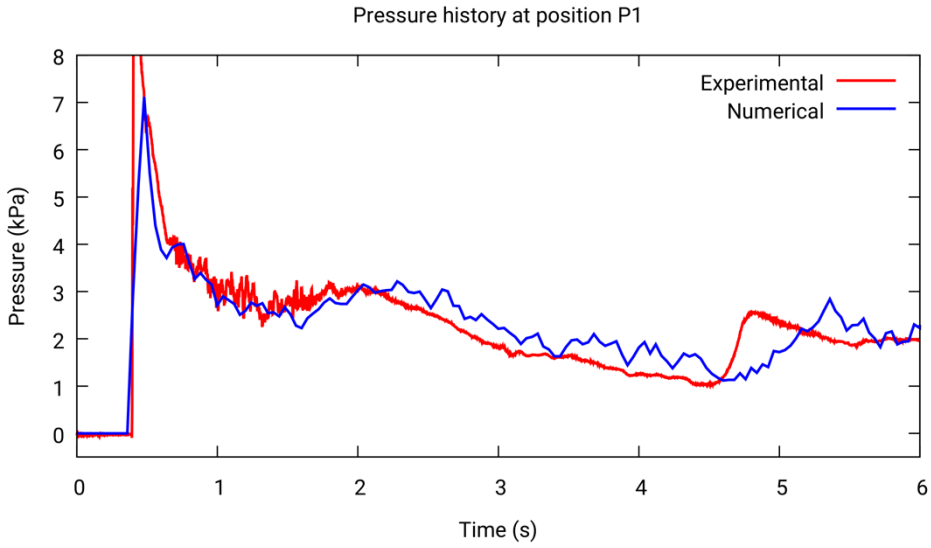

Fig.2: Pressure history on the front surface of the rigid box, comparison between experimental measurements and SPH simulation.

4.2 Automotive Water Wading

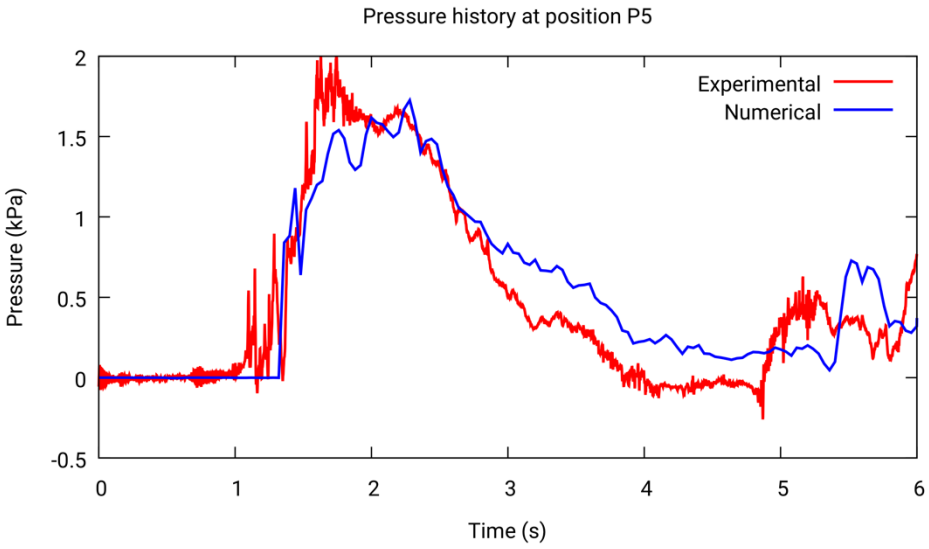

Fig.3: Pressure history on the top surface of the rigid box, comparison between experimental measurements and SPH simulation.

This second example represents a typical use case for this SPH formulation: an automotive water wading simulation. The problem setup is detailed in section 3. A vehicle is driven through a $10.0\ \mathrm{m} \times 2.4\ \mathrm{m} \times 0.4\ \mathrm{m}$ body of water, and the resulting fluid pressure acting on the front bumper is collected in two different locations. The interparticle distance used in the fluid domain of this simulation is $10\ \mathrm{mm}$, resulting in a total of roughly 13 million fluid and surface particles. A timestep of $\Delta t = 1\ \mathrm{ms}$ is employed for the entire run. The vehicle as an initial velocity of $2.5\ \mathrm{m.s^{-1}}$, while the front and rear tires have corresponding prescribed and initial velocities, respectively. A few snapshots of the simulation are given in Fig. 4, while the pressure obtained at two different locations of the front bumper are shown in Fig. 5. The boundary SPH particles sampling the vehicle are hidden for better visualization. A peak pressure is observed during the initial impact. Once the impact wave propagates away from the vehicle, the pressure sensor located on the top of the front bumper is above the water surface, which is reflected in the pressure diminishing to zero at this location. Validation of the method for this type of simulations is currently underway.

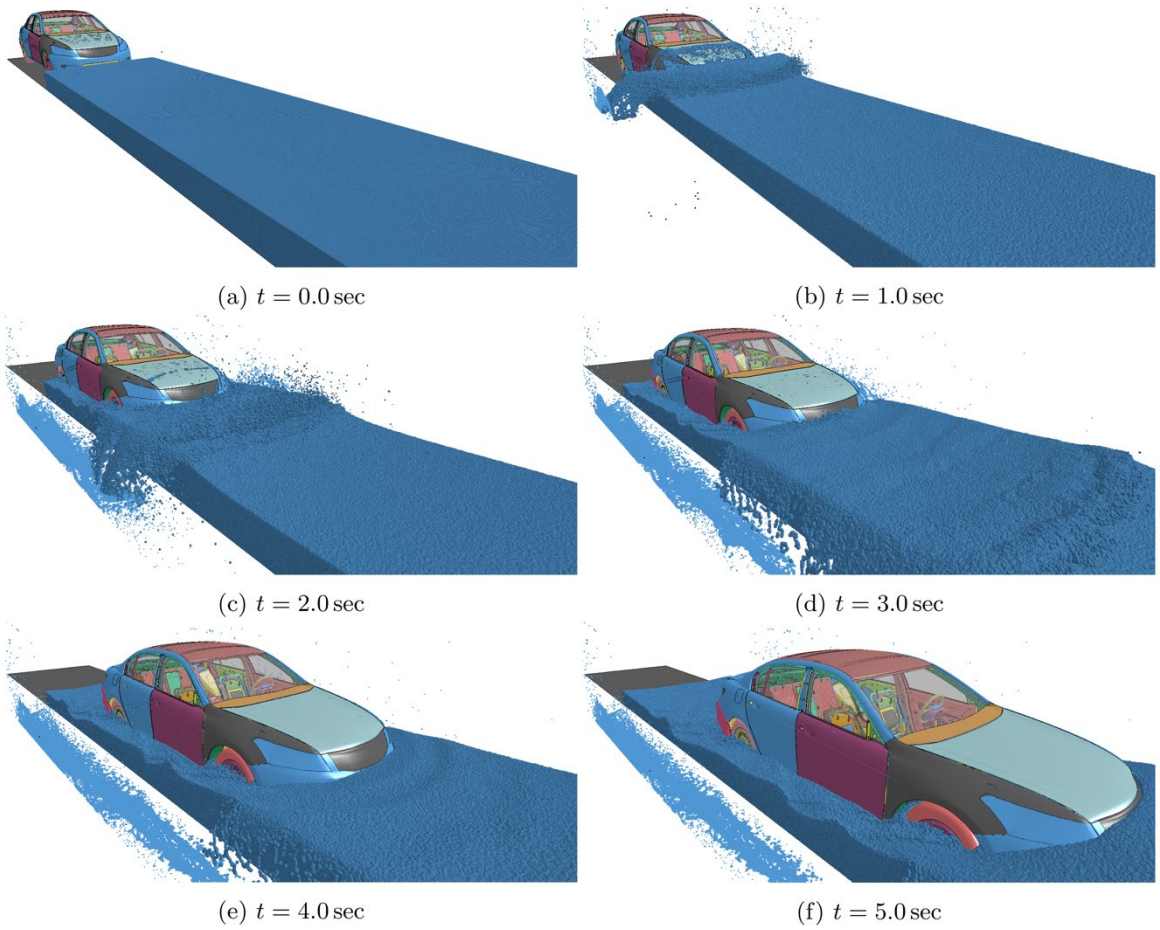

Fig.4: Automotive wading simulation.

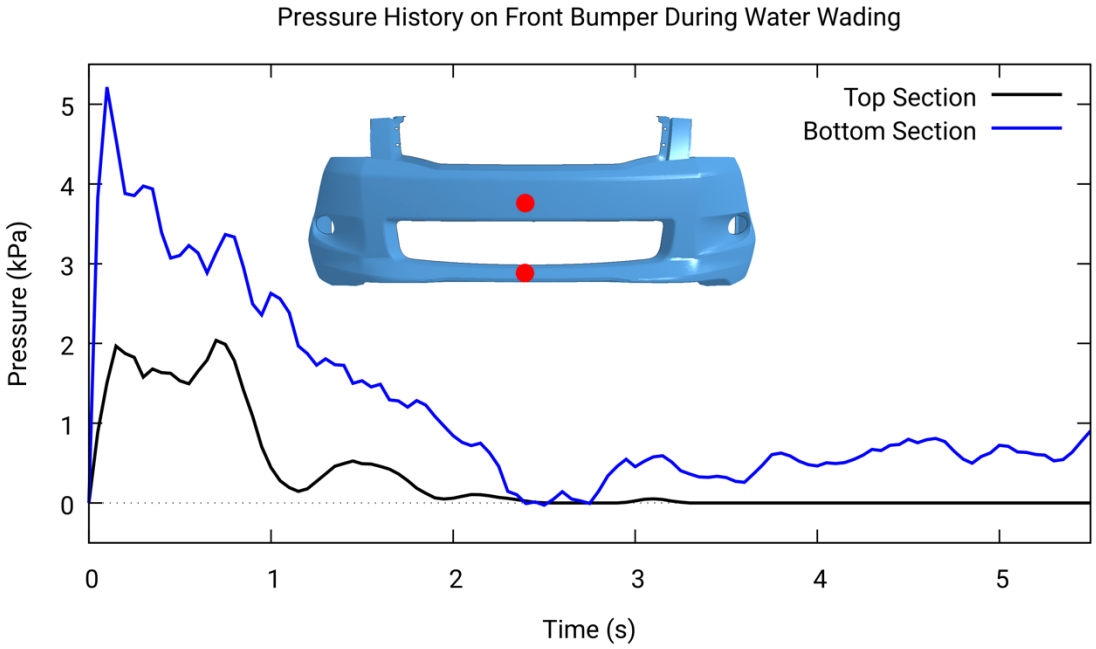

Fig.5: Pressure history on two locations of the front bumper.

5 Conclusion

An incompressible SPH formulation recently implemented in LS-DYNA was presented in this work. The semi-implicit nature of the method allows for larger time steps than typically available in SPH simulation while avoiding compromises on the incompressiblity of the fluid. The method is particularly suitable for large-scale water wading simulations, and can be employed for various water management problems that were previously unachievable in LS-DYNA due to very high computational cost. Preliminary testing shows good agreement between this new method and available experimental data and other numerical methods, but a more thorough validation study is still needed.

While the method is currently restricted to rigid structures, incorporating this technology into the existing implicit LS-DYNA solver is in progress. This would allow for modeling deformable structure without negatively impacting the time step, and greatly enhance the utility of this modeling tool for a broader spectrum of applications.

6 Litterature

[1] J Monaghan and Andrew Kos. “Solitary Waves on a Cretan Beach”. In: *Journal of Waterway Port Coastal and Ocean Engineering* 125 (May 1999).

[2] Diego Molteni and Andrea Colagrossi. “A simple procedure to improve the pressure evaluation in hydrodynamic context using the SPH”. In: *Computer Physics Communications* 180.6 (2009).

[3] Edouard Yreux. “Fluid Flow Modeling with SPH in LS-DYNA”. In: *Proceedings of the 15th International LS-DYNA Users Conference*. 2018.

[4] Moncho Gomez-Gesteira et al. “State-of-the-art of classical SPH for free-surface flows”. In: *Journal of Hydraulic Research* 48.sup1 (2010).

[5] Sharen J Cummins and Murray Rudman. “An SPH Projection Method”. In: *Journal of Computational Physics* 152.2 (1999).

[6] Markus Ihmsen et al. “Implicit incompressible SPH”. In: *IEEE Transactions on Visualization and Computer Graphics* 20.3 (2014).

[7] Alexandre Joel Chorin. “Numerical solution of the Navier-Stokes equations”. In: *Mathematics of computation* 22.104 (1968).

[8] Kamil Szewc, Jacek Pozorski, and J-P Minier. “Analysis of the incompressibility constraint in the smoothed particle hydrodynamics method”. In: *International Journal for Numerical Methods in Engineering* 92.4 (2012).

[9] Rui Xu, Peter Stansby, and Dominique Laurence. “Accuracy and stability in incompressible SPH (ISPH) based on the projection method and a new approach”. In: *Journal of computational Physics* 228.18 (2009).

[10] Songdong Shao and Edmond YM Lo. “Incompressible SPH method for simulating Newtonian and non-Newtonian flows with a free surface”. In: *Advances in water resources* 26.7 (2003).

[11] Larry D. Libersky et al. “Recent improvements in SPH modeling of hypervelocity impact”. In: *International Journal of Impact Engineering* 20.610 (1997).

[12] Nadir Akinci et al. “Versatile rigid-fluid coupling for incompressible SPH”. In: *ACM Transactions on Graphics* (TOG) 31.4 (2012).

[13] Nadir Akinci, Gizem Akinci, and Matthias Teschner. “Versatile surface tension and adhesion for SPH fluids”. In: *ACM Transactions on Graphics (TOG*) 32.6 (2013).

[14] Jason Wang. “LS-DYNA Automatic Re-Decomposition”. In: *Proceedings of the 12th European LS-DYNA Conference*. 2019.

[15] K.M.T. Kleefsman et al. “A Volume-of-Fluid based simulation method for wave impact problems”. In: *Journal of Computational Physics* 206.1 (2005).

[16] Eun-Sug Lee et al. “Application of weakly compressible and truly incompressible SPH to 3-D water collapse in waterworks”. In: *Journal of Hydraulic Research* 48.S1 (2010).